Toxicity of superparamagnetic iron oxide nanoparticles to the microalga *Chlamydomonas reinhardtii*

Jara Hurtado-Gallego, Gerardo Pulido-Reyes, Miguel González-Pleiter, Gorka Salas, Francisco Leganés, Roberto Rosal, Francisca Fernández-Piñas, Toxicity of superparamagnetic iron oxide nanoparticles to the microalga *Chlamydomonas reinhardtii*, Chemosphere, Volume 238, 2020, 124562, ISSN 0045-6535, https://doi.org/10.1016/j.chemosphere.2019.124562.

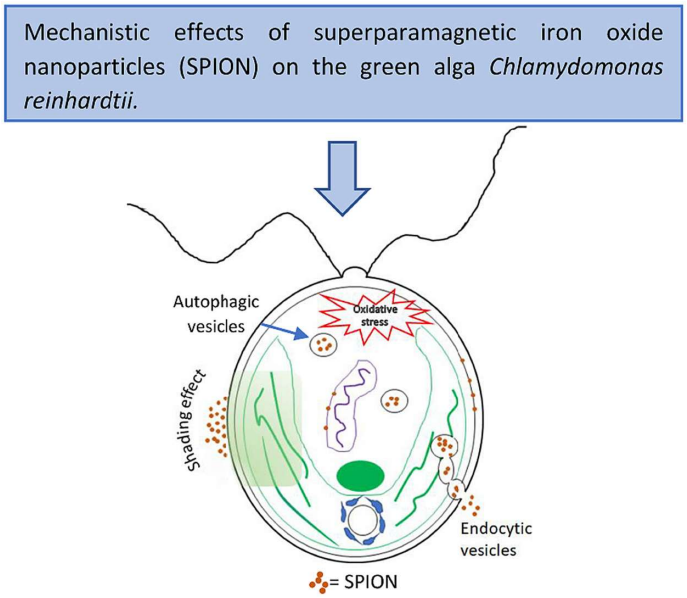

Toxicity of superparamagnetic iron oxide nanoparticles to the microalga *Chlamydomonas reinhardtii*

JaraHurtado-Gallego[1], Gerardo Pulido-Reyes[1], Miguel González-Pleiter[1], Gorka Salas[2], Francisco Leganés[1], Roberto Rosal[3] Francisca Fernández-Piñas[1,*]

[1] Departamento de Biología, Universidad Autónoma de Madrid, Cantoblanco, E-28049 Madrid, Spain

[2] IMDEA Nanociencia, C/Faraday 9, Cantoblanco, 28049 Madrid, Spain

[3] Departamento de Ingeniería Química, Universidad de Alcalá, E-28871 Alcalá de Henares, Madrid, Spain

[*] Corresponding author: francisca.pina@uam.es

Abstract

Superparamagnetic iron oxide nanoparticles (SPION) have been widely studied for different biomedical and environmental applications. In this study we evaluated the toxicity and potential alterations of relevant physiological parameters caused to the microalga *Chlamydomonas reinhardtii* (*C. reinhardtii*) upon exposure to SPION. The results showed dose-dependent toxicity. A mechanistic study combining flow cytometry and physiological endpoints showed a toxic response consisting of a decrease in metabolic activity, increased oxidative stress and alterations in the mitochondrial membrane potential. Additionally, and due to the light absorption of SPION suspensions, we observed a significant shading effect, causing a marked decrease in photosynthetic activity. In this work, we demonstrated for the first time, the internalization of SPION by endocytosis in *C. reinhardtii*. These results demonstrated that SPION pose a potential risk for the environment if not managed properly

Keywords: Microalgae; SPION; Toxicity mechanisms; Shading effect; Internalization

1. Introduction

The technologies based on nanoparticles (NPs) have increased in the last years with the advent of a huge variety of products for many different applications (Bundschuh et al., 2018). Superparamagnetic iron oxide nanoparticles (SPION) are among the most used NPs in biomedical fields as contrast agents for magnetic resonance imaging, drug delivery systems or as hyperthermia agents in cancer therapies (Mosayebi et al., 2017). SPION are usually formed by a mineral core of a magnetic element or in combination with more magnetic elements such as nickel, cobalt or their oxides, and an organic coating, such as dextran, polyethylene glycol, poly (vinylpyrrolidone), streptavidin, and meso-2,3-dimercaptosuccinic acid (DMSA) among others (Mosayebi et al., 2017). Due to their adsorptive capabilities, SPION have been proposed as an environmentally benign method for contaminated site remediation (Gutierrez et al., 2017; Khin et al., 2012; Mosayebi et al., 2017; Tang and Lo, 2013; Truskewycz et al., 2018). SPION have been used to remove arsenic (Yavuz et al., 2006), polycyclic aromatic compounds (Zhang et al., 2010) or heavy metals (Ambashta and Sillanpää, 2010; Cui et al., 2013; Hu et al., 2005; Matei et al., 2016; Sheikh, 2013). The efficiency of SPION can be enhanced by proper surface modification (Tong et al., 2011; Zhang and Elliott, 2006). In this regard, one of the advantages of using SPION is that the purification process to regenerate these NPs does not produce secondary waste, allowing their reuse in environmental remediation (Gutierrez et al., 2017).

Due to their biocompatibility and low cytotoxicity, SPION are considered safe for biomedical use (Fadeel and Garcia-Bennett, 2010; Gholami et al., 2015; Laffon et al., 2018; Singh et al., 2010). To date, there are a variety of studies about the toxicity of SPION in different cell lines and no clear toxicity has been found (Fadeel and Garcia-Bennett, 2010; Gholami et al., 2015; Saptarshi et al., 2013; Singh et al., 2010). However, the evaluation of their effects on environmental organisms has not been fully addressed and, at the same time, their expanding use supposes an environmental risk that needs proper assessment (Tang and Lo, 2013). In this context, only a few works have studied the toxicological effects of SPION. Wu et al. (2012) (Wu et al., 2012) studied the biological effects of dimercaptosuccinic acid (DMSA) coated nano-Fe_2O_3 to the nematode *Caenorhabditis elegans* finding that these NPs decreased its growth and reproduction and induced ROS formation. Barhoumi et al. (2015) used the aquatic plant *Lemma gibba* as model organism to test the toxicity of SPION finding growth inhibition, ROS formation, decrease in chlorophyll content and photosynthesis inhibition. The toxicity of nano-Fe_3O_4 and nano-Fe_2O_3 has been studied in the microalgae *Chlorella vulgaris* (*C. vulgaris*) (Barhoumi and Dewez, 2013; Chen et al., 2012b), *Pseudokirchneriella subcapitata* and in the cladoceran *Daphnia magna* (Llaneza et al., 2016), these NPs caused ROS formation and deterioration of photosynthetic activities in the

algae and inhibition of division rate in Daphnia. Although different parameters were measured, the authors were mostly interested in describing these effects in a range of NP concentrations rather than in establishing mechanistic links between the measured functions and thus, more studies aimed at understanding the toxic mechanisms of SPION in aquatic environments are needed.

In this study, we used two SPION based on synthetic γ-Fe_2O_3 (maghemite) or Fe_3O_4 (magnetite) nanomaterials with DMSA coating. We performed a physicochemical characterization of SPION particles and suspensions and evaluated their biological effects and toxic mode of action towards *C. reinhardtii*. This aquatic organism is a unicellular biflagellate microalga used as model organism in many nanotoxicological studies (Martín-de-Lucía et al., 2018; Navarro et al., 2008; Wang et al., 2008). In particular, we studied reactive oxygen species (ROS) formation, photosynthetic efficiency, physiological alterations and nanoparticle internalization after SPION exposure trying to provide novel information on the toxicological mechanisms of SPION on primary producers in aquatic environments.

2. Materials and methods

2.1. Synthesis of SPION

SPION with average core size of 8 nm (*IO8*) were synthesized by a thermal decomposition route, inspired in the method reported by Sun et al. (2004) (Sun et al., 2004) and Pacakova et al. (2017). The reaction was carried out under mechanical stirring and nitrogen flow. Briefly, $Fe(acac)_3$ (10 mmol; acac = acetyl acetonate), oleic acid (30 mmol) and 1,2-dodecanodiol (20 mmol) were dissolved in 1-octadecene (100 mL). The mixture was heated at a rate of 2 °C/min to 100 °C and kept at that temperature for 1 h to degas it. Then, it was heated up again (2 °C/minute) to 190 °C. The temperature was kept for 2 h and heated again to reflux at 3 °C/minute. After 30 min at reflux temperature, the mixture was allowed to cool down to room temperature and washed several times with ethanol, centrifuged and SPION isolated with the aid of a magnet.

SPION with average core size of 16 nm (*IO16*) were synthesized by thermal decomposition of an iron oleate complex (10 mmol) in 1-octadecene (100 mL) in the presence of oleic acid (5 mmol) under nitrogen flow following previously reported procedures with minor variations (Park et al., 2004; Salas et al., 2012). Briefly, the mixture was heated at 2 °C/minute (with mechanical stirring only until 60 °C) up to 210 °C. The reaction was kept at that temperature for 1 h and heated again to reflux at 3 °C/minute. After 1 h, the mixture was allowed to cool down to room temperature and washed several times with ethanol, centrifuged and SPION recovered using a magnet. In both cases, the obtained SPION are hydrophobic and need surface modification to make them dispersible in aqueous medium. Surface modification was carried out with DMSA through a ligand exchange procedure as previously described by Salas et al. (2012) (Salas et al., 2012).

2.2. Physicochemical characterization of SPION

Particle size was examined by transmission electron microscopy (TEM) in a JEOL JEM 1010 microscope operating at 100 kV. The size distributions were determined through manual analysis of ensembles of over 300 particles found in randomly selected areas of the enlarged micrographs, with Imagetool software to obtain the mean size and standard deviation.

Curves of sample magnetization (M) *vs.* external magnetic field (H) were collected between −20000 and 20,000 Gauss in a vibrating sample magnetometer (VSM). Both types of nanoparticles exhibit superparamagnetic behaviour before and after contact with the cells. After incubation with microalgae during 72 h, the SPION and the microalgae were filtered by glass microfiber filter Whatman with a loading capacity of 1.6 μm, holding back the cells and the NPs internalized or attached to the cells.

Hydrodynamic diameter and ζ-potential of the SPION suspensions were measured at 10 mg/L (pH 7) in ultrapure water and in TAP/6 culture medium by dynamic light scattering (DLS) and electrophoretic light scattering respectively using a Zetasizer Nano SZ analyser from Malvern Instruments. Measurements were essentially as described elsewhere (Gonzalo et al., 2014).

2.3. Microalgal cultures and bioassays

C. reinhardtii Dangeard (strain CCAP 11/32 mt^+) is a unicellular green alga obtained from the Culture Collection of Algae and Protozoa of Dunstaffnage Marine Laboratory (Scotland, UK). Cells were routinely grown in 250 mL flasks on a rotatory shaker at 135 rpm in TAP modified (TAP/6) culture medium (pH 7) under controlled conditions: 28 °C with continuous illumination at 60 μmol photons m^2 s^{-1}. The TAP/6 growth medium was modified from TAP growth medium (Hoober, 1989) by diluting it 6 times in ultrapure water to reduce its conductivity and increase the stability of SPION as previously reported (von Moos et al., 2015). Table S1 shows the specific growth rate (μ, h^{-1}) and generation time (g, h) calculated as described by Arana et al.,(2019). As can be seen, after 72 h of culture, growth rate of the alga in TAP/6 medium is inhibited by 20% when compared with growth in TAP, shifting from a generation time of around 28 h in TAP to around 35 h in TAP/6. Thus, the dilution slightly affected the normal growth of *C. reinhardtii* but did not cause any deleterious effect in cell viability (as measured by integrity of cell membrane) as shown by fluorescent propidium iodide flow cytometry analysis (see Fig. S1).

Exposure experiments were carried out in 14 mL TAP/6 culture medium in 25 mL flasks with different concentrations of SPION (0–100 mg/L) from a stock of

2300 mg/L in MilliQ water following OECD guideline TG 201. Optical density at 750 nm (OD_{750nm}) was measured using a Synergy HTmulti-mode microplate reader (BioTek, USA). Toxicity was expressed as EC_{50} (the effective concentration that caused 50% growth inhibition with respect to a non-treated control). All the bioassays were performed at least in triplicate after 72 h exposure at the EC_{50} of each SPION.

2.4. ROS formation and lipid peroxidation

Intracellular ROS produced by *C. reinhardtii* were measured by using the cell permeable fluorescent fluorochrome 2′7′-dichlorodihydrofluorescein diacetate (H_2DCFDA, Invitrogen Molecular Probes, Thermo Fisher) as previously described by Rodea-Palomares et al. (2010) (Rodea-Palomares et al., 2010). The emitted fluorescence of fluorochromes (488 and 530 nm) was measured after 72 h of exposure on a Synergy HT multi-mode microplate reader (BioTek, USA). Results were normalized by measuring *in vivo* fluorescence of chlorophyll *a* of the sample as described elsewhere (Rodea-Palomares et al., 2012).

Lipid peroxidation was determined *in vitro* after the formation of malondialdehyde (MDA), a by-product of lipid peroxidation that reacts with thiobarbituric acid reactive substances (TBARS) following the protocol described elsewhere with minor modifications (Elbaz et al., 2010; Ortega-Villasante et al., 2005). Briefly, *C. reinhardtii* was centrifuged for 5 min at 4500 rpm and submerged in liquid nitrogen. Frozen pellets were homogenized in 0.5 mL of TCA-TBA-HCl reagent (15% w/v) composed by trichloroacetic acid, TCA, 0.37% (w/v), 2-thiobarbituric acid, TBA, 0.25 M HCl, and 0.01% butylated hydroxytoluene. Absorbance was measured at 535 and 600 nm on a Synergy HT multi-mode microplate reader (BioTek, USA) using 96-well transparent microplates. The amount of TBARS was calculated by using the extinction coefficient of 155 $mM^{-1}cm^{-1}$. Lipid peroxidation was expressed as TBARS nmol g^{-1} dry weight (DW). DW was calculated from the OD_{750nm} as previously described by Berberoglu et al. (2008) (Berberoglu et al., 2008).

2.5. Flow cytometry analyses

Flow cytometry analyses of *C. reinhardtii* after SPION exposure were carried out on a Cytomics FC500 MPL flow cytometer fitted with an argon-ion excitation laser (488 nm), a forward scatter detector (FS), a side scatter detector (SS) and four fluorescence detectors: FL1 (505-550 nm), FL2 (550–600 nm), FL3 (600-645 nm) and FL4 (>645 nm; used to estimate cell chlorophyll *a* content). Five physiological parameters were analysed by FCM (Table 1): membrane integrity (PI), cytoplasmic membrane potential (DiBAC4(3)), non-specific esterase activity (FDA), intracellular pH (BCECF-AM) and mitochondrial membrane potential (JC-1). The fluorochrome concentrations and incubation times used were as previously reported by Prado et al. (2012) (Prado et al., 2012), González-Pleiter et al., 2017 (González-Pleiter et al., 2017) and Tamayo-Belda et al., 2019 (Tamayo-Belda et al., 2019) and can be found in Table 1. After 72 h of exposure to the EC_{50} of each SPION, cells were incubated with each fluorochrome at room temperature in the dark prior to flow cytometry analyses. At least three independent experiments with triplicate samples were performed for each parameter and at least 5000 cells were analysed using the Flowing software version 2.5 (Cell Imaging Core, Turku Centre for Biotechnology).

2.6. Oxygen evolution, chlorophyll content and shading effect

Oxygen evolution was measured at 28 °C under saturating white light (300 μmol photons m^{-2} s^{-1}) as

Table 1. Concentrations and incubation times of the fluorochromes used in the flow cytometry analysis in this study.

Fluorochrome	Acronym	Physiological parameter	Final concentration (μg mL^{-1})	Incubation time (min)	References
Propidium iodide	IP	Membrane integrity	5	10	González-Pleiter et al., 2017; Prado et al., 2012; Tamayo-Belda et al., 2019
bis-(1,3-dibutylbarbituric acid) trimethine oxonol	DiBAC4(3)	Cytoplasmic membrane potential	2.5	10	González-Pleiter et al., 2017; Prado et al., 2012; Tamayo-Belda et al., 2019
Fluorescein Diacetate	FDA	Non-specific esterase activity	2.5	15	González-Pleiter et al., 2017; Prado et al., 2012; Tamayo-Belda et al., 2019
20,70-bis(2-carboxyethyl)-5(6)-carboxy fluorescein	BCECF	Intracellular pH	5	40	González-Pleiter et al., 2017; Prado et al., 2012; Tamayo-Belda et al., 2019
Tetraethylbenzimidazolyl-carbocyanine iodide	JC-1	Mitochondrial membrane potential	5	20	González-Pleiter et al., 2017; Prado et al., 2012; Tamayo-Belda et al., 2019

previously described using a Hansatech Clark-type electrode by Leganés et al. (2014) with a Clark-type oxygen electrode (Hansatech). Briefly the cells were supplemented with 5 mM $NaHCO_3$, pH 7.5, and photosynthetic rates were related to total chlorophyll *a* content.

For chlorophyll content determinations, culture aliquots were extracted in methanol (90%, w/v) at 4 °C for 24 h in darkness. Chlorophyll *a* as well as total chlorophyll content of the extract (chlorophyll *a*+b) were determined according to the spectrophotometric method of Ahmed (2016) (Ahmed, 2016).

To test the shading effect of SPION suspensions, double layer glass arrangements were prepared by introducing 25 mL flasks into 100 mL beakers (Fig. S2). For shading controls, the outer beaker was filled with 35 mL of algal growth medium (transparent) and the inner flask contained the algal cells. To evaluate the potential shading effect of SPION, the concentration corresponding to their EC_{50} was added in the outer beaker. The growth of algal cells in the inner flask was compared to the same result when the outer volume was filled with algal growth medium (transparent). This experimental simulated the shading effect of SPION avoiding their direct contact with microalgae (Aruoja et al., 2009).

2.7. SPION-alga interaction (TEM analyses)

For TEM micrographs, *C. reinhardtii* cells were exposed to the calculated EC_{50} of each SPION for 72 h. Non-exposed cells (control) and exposed cells were collected by centrifugation, washed three times in phosphate buffer 0.1 M, pH 7.2 for 10 min, and then fixed using 4% paraformaldehyde and 2.5% glutaraldehyde in phosphate buffer for 4 h at 4 °C. The samples were subsequently rinsed three times with phosphate buffer and stored at 4 °C overnight. Post fixation was performed on 1 mm of 2% agar. After post fixation process, the samples were rinsed with phosphate buffer three more times and dehydrated through a graded acetone series of 30-50-70-80-90-95-100% for 15 min. Infiltration and embedding of Spurr-resin was conducted by increasing resin concentrations in acetone (25%, 50%, 75% and 100%). The samples were subsequently embedded in pure resin at room temperature overnight. Finally, resin polymerization took place at 60 °C for 48 h. The sectioned samples in semi-thin (0.5 μm) and ultra-thin sections (60 nm) were stained with uranyl acetate and lead citrate. Ultrathin sections were visualized on a JEOL (JEM 1010) electron microscope (100 kV) or on a JEOL JEM 1400 (100 kV) coupled with XEDS (X-Ray Energy Dispersive Spectroscopy). All reagents used for TEM preparations were Electron Microscopy grade.

2.8. Statistical analysis

All data were obtained from a minimum of three independent experiments with three replicates for each assay condition. All test of statistically significant differences between data sets were performed using Student's *t*-test and one-way analysis of variance (ANOVA) which were computed using R analysis Rcdmr package (R for windows, 3.0.2 copyright© The Foundation for Statistical Computing).

3. Results and Discussion

3.1. Physicochemical characterization of SPION

The average core size of both SPION, IO8 and IO16, was determined by TEM micrographs. The values are given in Table 2. Representative TEM images are also shown in Fig. 1 A and D. The characteristics of DMSA-coated suspensions of IO8 and IO16 in distilled water and TAP/6 medium are also indicated in Table 2. Both IO8 and IO16 formed stable suspensions with hydrodynamic sizes ranging from 59 to 79 nm both in distilled water and TAP/6 medium. The colloidal stability was higher for IO16 (ζ-potential −27.1 mV) than for IO8 (ζ-potential −18 mV) suspensions. Further information about their physicochemical behaviour along time is summarized in Table S2, where it can be observed that the SPION tended to aggregate with time.

After the incubation with the microalgae for 72 h, the superparamagnetic behaviour is preserved and no apparent change could be observed (Fig. 1C and F), which means that, from the point of view of the magnetization, no degradation of the SPION has occurred under these conditions.

3.2. Toxicity of SPION to *C. reinhardtii*

The effect of SPION on *C. reinhardtii* growth was assessed by measuring the OD_{750nm}. The results of the exposure to IO16 and IO8 in the concentration range of 0.5–100 mg/L are shown in Fig. 2. Both SPION caused algal growth inhibition that was significant ($p < 0.01$) for concentrations higher than 10 mg/L, showing similar concentration-response profiles (Fig. 2). The EC_{50} for IO16 was 75 ± 5 mg/L and the EC_{50} of IO8 that was 100 ± 4 mg/L. More toxicity parameters (the EC_{10} and EC_{20}) for both SPION are shown in Table S3. The

Table 2. Physicochemical properties of the tested SPION in ultrapure water and in TAP/6 medium.

Particle	Size ± s. d. from TEM (nm)	Ultrapure H_2O	TAP/6 medium	ζ- potential (mV)	Hydodynamic diameter (nm)	PDI
IO16	16 ± 2	−39.1 ± 9.7	78.5 ± 0.5	−27.1 ± 1.1	61.6 ± 0.7	0.2
IO8	7.6 ± 0.9	−16.7 ± 2.3	63.2 ± 1.1	−18.0 ± 2.5	59.6 ± 8.5	0.4

[a]PDI: Polydispersity index

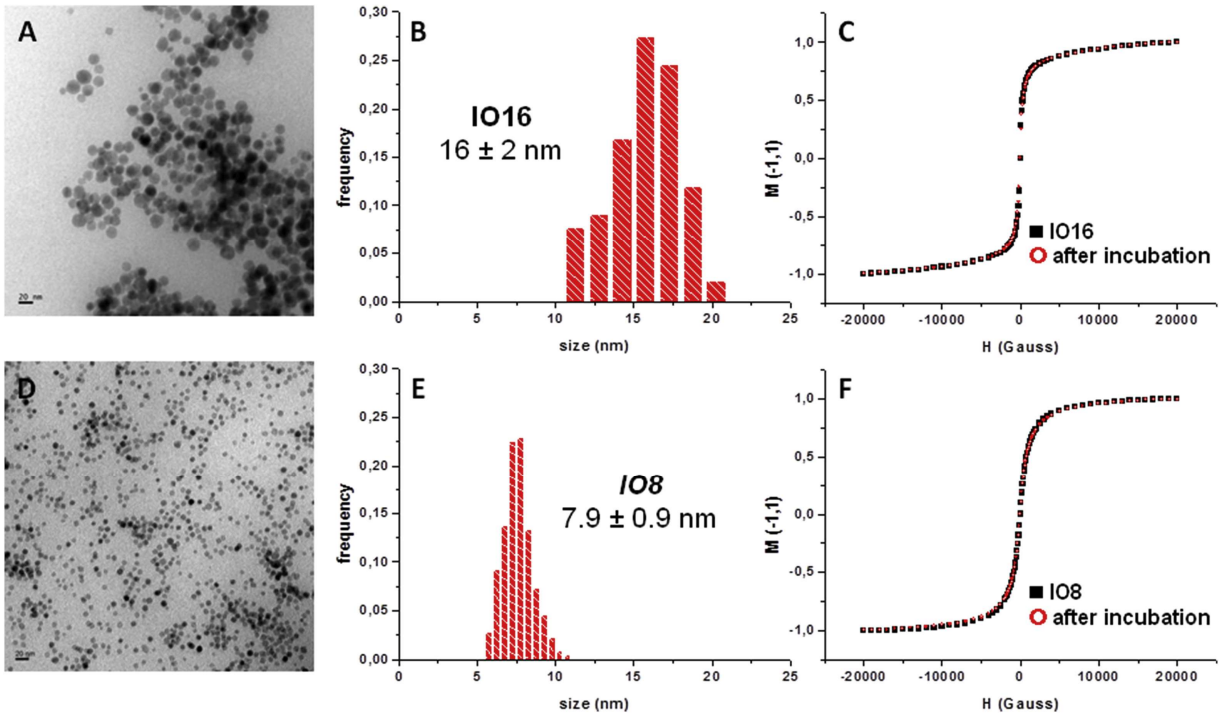

Figure 1. Selected TEM micrographs and histograms with mean size and standard deviation of IO16 (A, B) and IO8 (D, E). C and F show the magnetization M(H) curves of IO16 (C) and IO (F) before (■) and after (o) incubation with the cells.

toxicity of nano-Fe_3O_4 SPION to the plant *Lemma gibba* and to the alga *Chlorella vulgaris* was tested and found non-toxic, with most endpoints in the hundreds of mg/L range (Barhoumi and Dewez, 2013; Barhoumi et al., 2015). No other studies have been found on the effect of SPION to photosynthetic organisms. Our data showed that *C. reinhardtii* is relatively sensitive to SPION and, therefore, suitable for the evaluation of the environmental risks of them. It is interesting to note that at low concentrations we observed a certain growth stimulation or hormetic effect, although not statistically significant ($p > 0.001$). A similar hormetic effect was found by Llaneza et al. (2016) in their study of the toxic effects of nano-Fe_3O_4 and nano-Fe_2O_3 on *Pseudokirchneriella subcapitata* and *Daphnia magna* (Llaneza et al., 2016), particularly at the lower concentrations tested. A suitable explanation for that could be that it is due to a nutrient effect as Fe is an essential element and there is some dissolution of Fe from the NPs (although negligible, otherwise there should be differences in the magnetization curves, see Fig. 1C and F). At the highest concentrations tested, hormesis is not present as toxicity is already found. Nevertheless, hormesis is difficult to explain, although evidence is gathering that most chemicals, which are toxic at high concentrations, may have stimulatory effect in an organism when applied at low concentrations (Calabrese and Baldwin, 2001). There are intense scientific debates regarding interpretation of these observations: some authors believe that hormesis is a general stress response to any chemical that, somehow, preconditions and protects cells against the subsequent toxicity resulting from a higher dose of the same chemical (Calabrese, 2016; Calabrese and Baldwin, 2001; Stebbing, 1997). Other authors consider that hormesis is not a real phenomenon (Forbes, 2000; Parsons, 2003). Deryabin and Aleshina (2008) (Deryabin and Aleshina, 2008) found a stimulatory effect of some salts such as chlorides and sulphates on the luminescence response of *Photobacterium phosphoreum* and recombinant *Escherichia coli* with cloned *luxCDABE* genes of *Photobacterium leiognathi* 54D10, which could also be attributable to a nutrient effect.

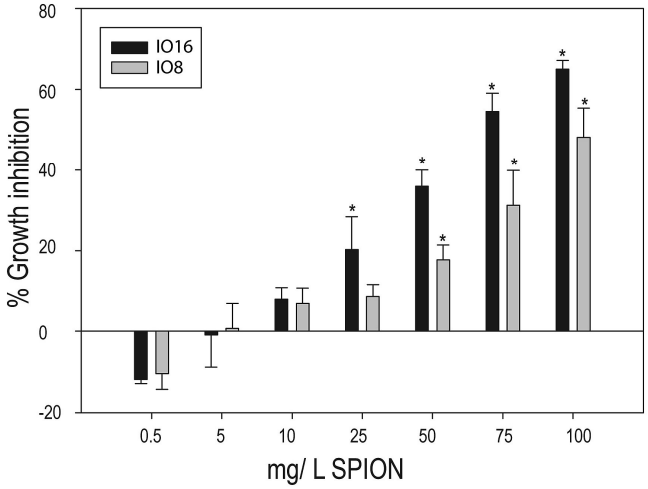

Figure 2. Effect of 72 h of exposure to SPION on growth of *C. reinhardtii*. Data are expressed as percentage of the value of untreated cells (mean ± standard deviation). Asterisks mark statistically significant ($p < 0.001$) differences.

3.3. SPION induce ROS formation in *C. reinhardtii*

Oxidative stress is one of the main mechanisms by which NPs impair bacteria and microalgae (Gonzalo et al., 2014; Pulido-Reyes et al., 2015; von Moos and Slaveykova, 2014). We recorded changes in ROS formation by means of the intracellular fluorescent dye

H_2DCFDA after 0.5, 24 and 72 h of exposure to Ec_{50} SPION concentrations (see Fig. 3; the raw fluorescence data are shown in Fig. S3). After 30 min of the exposure to Ec_{50} of SPION no increase in ROS formation was observed. Interestingly, ROS formation after 30 min was lower for IO8 and IO16 than for unexposed cells. This could be due to the lower metabolic formation of ROS because of the shading phenomenon. However, this hypothesis was tested, and shading did not have any significant effect on ROS formation (Fig. S4, where the effect of shading was tested in cells exposed during 30 min to IO16, which is the SPION that clearly caused shading effect on photosynthesis, see below). After 24 h of exposure, ROS formation increased and was significantly higher than controls even after 48 and 72 h (Fig. 3). Other studies with SPION have also reported an increase in the oxidant species in *C. vulgaris* (Barhoumi and Dewez, 2013).

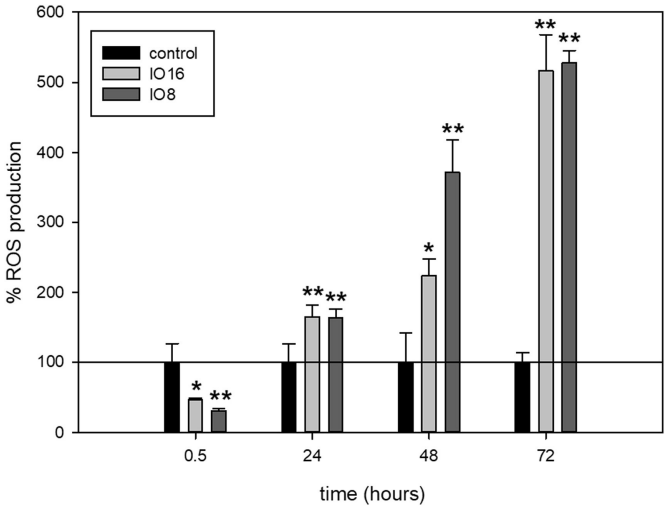

Figure 3. Effect of SPION on intracellular ROS production of *C. reinhardtii* cells using the fluorochrome H_2DCFDA after 0.5, 24, 48 and 72 h of exposure. Results are presented as percentage ± SD with respect to control (100% as indicated by the solid line). Asterisks indicate statistically significant (*p< 0.05 and **p < 0.001) differences.

ROS may produce lipid peroxidation starting by the removal of hydrogen from an unsaturated fatty acid chain and further reaction with oxygen to generate lipid peroxyl radicals (Ševcu AEl-Temsah et al., 2009). Lipid peroxidation occurs as a normal process in aerobic organisms but during stress conditions, it could damage the membrane, increasing membrane permeability (von Moos and Slaveykova, 2014). Fig. 4 shows that after 72 h of exposure, both SPION significantly increased lipid peroxidation. The analysis was performed by quantification of TBARS (thiobarbituric acid reactive substances) that are end products of lipid peroxidation, predominantly malondialdehyde. Both NPs led to membrane lipid peroxidation (measured as MDA concentration): over 1700% in the case of IO16 ($p < 0.001$) and over 500% ($p < 0.005$) for IO8 in comparison with control cultures. Previous studies have observed lipid peroxidation in algae and cyanobacteria after the exposure to NPs for 72 h: TiO_2 NPs in *Chlamydomonas reinhardtii* (Chen et al., 2012a; Wang et al., 2008); Fe_3O_4 on *Chlorella vulgaris* (Chen et al., 2012b) and cationic G5 and G7 PAMAM dendrimers in the cyanobacterium *Anabaena* sp. PCC7120 (Tamayo-Belda et al., 2019).

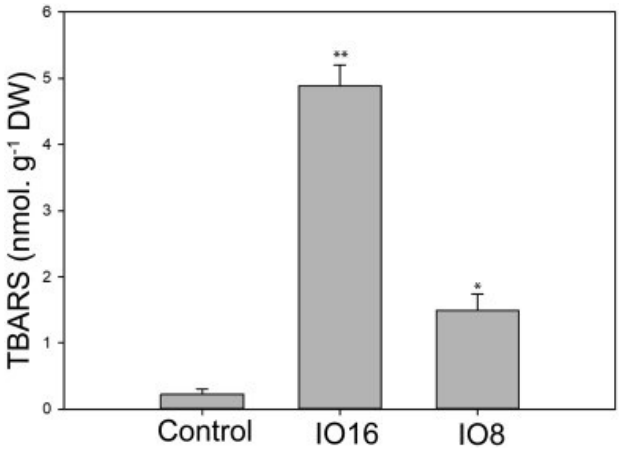

Figure 4. Lipid peroxidation levels as relative content of TBARS (nmol g^{-1} DW) of *C. reinhardtii* exposed to SPION during 72 h of exposure. Asterisks indicate statistically significant (*p < 0.05 and **p < 0.001) differences.

3.4. SPION altered several physiological parameters of *C. reinhardtii*

Intracellular ROS and lipid peroxidation induce damage in cytoplasmic membrane and internal organelles. We specifically tested cytoplasmic and mitochondrial membrane potential, intracellular pH and metabolic activity using flow cytometry. This technique allows the rapid and quantitative measurement of individual cells responses to a toxic stress. Fig. 5 shows the results of the physiological evaluation of algal cells exposed to IO16 and IO8 at their Ec_{50}. Representative histograms and dot plots can be found as Supplementary Material Fig. S5.Peroxidised membranes change their permeability and, under extreme conditions lose their integrity (Ševcu AEl-Temsah et al., 2009). The effect of SPION on the cytoplasmic membrane potential of *C. reinhardtii* was studied using the fluorescent dye $DIBAC_4(3)$. Fig. 5 A shows a significant ($p < 0.005$) increase of membrane hyperpolarization in the case of IO16 after 1 and 24 h of exposure. However, no significant alteration in the cytoplasmatic membrane potential was observed for longer times. In the case of IO8, no relevant alteration was observed (Fig. 5 A). To check membrane integrity, the fluorescent dye propidium iodide (PI) was used since it is unable to pass through intact cell membranes (PI−). However, when the integrity of the cell membrane fails, PI is able to enter and stain nucleic acids (PI+), allowing one to discriminate between those cells that emit fluorescence and therefore present damage in the cytoplasmic membrane and those in which the fluorochrome does not penetrate and no fluorescence is emitted and, therefore, cells maintain the integrity of the membrane.

Fig. S1 shows the PI fluorescence histograms of SPION-treated cells with respect to the non-treated control cells. No PI + cells were found, indicating no relevant damage of the integrity of the cytoplasmic membrane in SPION-exposed cells.

Mitochondria have also been reported as highly important in environmental stress caused by pollutants (González-Pleiter et al., 2017) and are also subject to lipid peroxidation. We measured potential mitochondrial dysfunction in *C. reinhardtii* caused by SPION with the fluorescent fluorochrome JC-1. Fig. 5 B shows the results of the mitochondrial membrane potential of the cells after the exposure to the EC_{50} of each SPION. After 1 h of exposure to IO8, a dramatic mitochondrial membrane potential depolarization ($p < 0.001$) was observed (around 80% reduction with respect to the control) maintained throughout the 72 h experiment. After exposure to IO16, *C. reinhardtii* cells presented a gradual mitochondrial membrane potential depolarization increasing over time with maximum

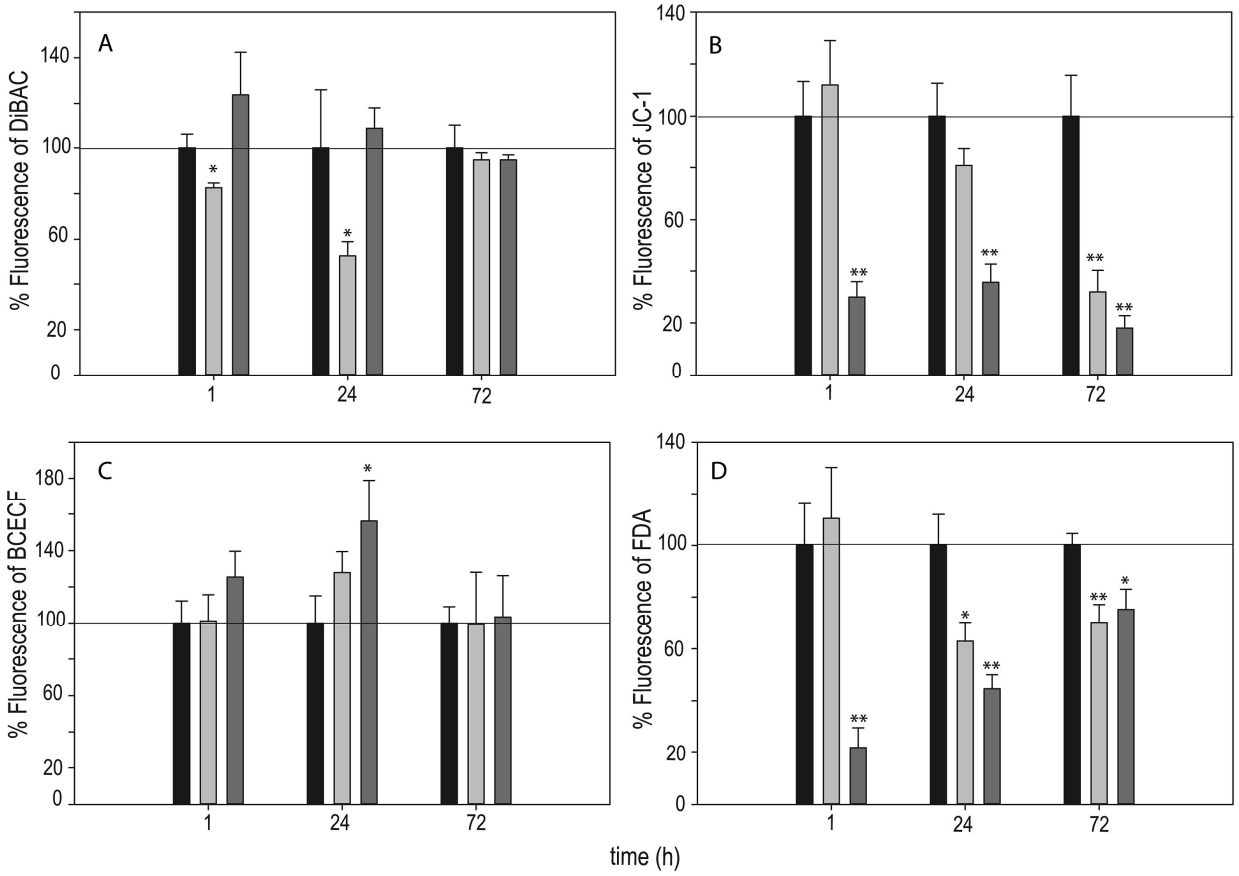

Figure 5. Alterations on relevant parameters of *C. reinhardtii* after 1, 24 and 72 h of exposure to SPION as measured by flow cytometry using different fluorochromes: (A) plasma membrane potential, (B) mitochondrial membrane potential, (C) intracellular pH and (D) metabolic activity. Control (■), IO16 (▭) and IO8 (▭). Results are shown as percentage of variation of each parameter with respect to control (100% as indicated by the solid line). Asterisks indicate statistically significant (*$p < 0.05$ and **$p < 0.001$) differences. (See also Fig. S5).

depolarization after 72 h of exposure (significant at $p < 0.001$). It has been previously reported that different NPs could depolarize the mitochondrial membrane of *C. reinhardtii* (Martín-de-Lucía et al., 2018; Xia et al., 2006), but this is the first time that depolarization in the mitochondrial membrane potential is found in a microalga after exposure to SPION.

To evaluate changes in the intracellular pH, we used the green/red fluorescence ratio of BCECF dye that increases when intracellular pH increases and decreases when it decreases. Fig. 5C shows a significant ($p < 0.05$) alkalinisation of the cytoplasm at 24 h caused by IO8. pH values recovered at longer exposure times (72 h). The alkalinisation of cytoplasm at shorter exposure times has been correlated with oxidative stress in microalgae exposed to metals (Cid et al., 1996). In *C. reinhardtii,* this cytoplasmic alkalinisation has been observed in cells exposed to organic pollutants like triclosan (González-Pleiter et al., 2017) or paraquat (Prado et al., 2012).

The fluorescent dye FDA was used to study the metabolic activity based on the measure of non-specific esterases activity of *C. reinhardtii* (Prado et al., 2012) after 1, 24 and 72 h of exposure to SPION at their Ec_{50} concentration. Fig. 5 D shows a drastic and significant ($p < 0.001$) decrease of esterase activity following the exposure to IO8. However, after the exposure to IO16 the metabolic activity of the cells showed a significant ($p < 0.001$) decrease only after 24 h. After 72 h of exposure to both NPs, the cells showed a decrease of

esterase activity to around 60% of the control. A decrease of esterase activity has been reported before for *C. reinhardtii* after exposure to different pollutants such as triclosan or atrazine (Esperanza et al., 2015; González-Pleiter et al., 2017) indicating decreased in metabolic activity. A decrease of esterase activity was also observed in *C. reinhardtii* after exposure to graphene oxides (Martín-de-Lucía et al., 2018).

3.5. Photosynthetic response of *C. reinhardtii* to SPION and shading effect

The decrease of metabolic activity has been previously correlated with a decrease of the photosynthetic activity in unicellular microalgae (Brookes et al., 2000). To check potential oxidative damage of SPION to photosynthesis, we studied the photosynthetic activity of the cells after exposure to both SPION as O_2 evolution. The decrease of photosynthetic activity of *C. reinhdartii* upon exposure to different toxicants has been reported elsewhere (Prado et al., 2012; Esperanza et al., 2015; Chen et al., 2012a; González-Pleiter et al., 2017; Navarro et al., 2015; Saison et al., 2010). Specifically concerning SPION, a negative effect towards photosynthetic activity of *C. vulgaris* and *Lemma gibba* was reported before (Barhoumi and Dewez, 2013; Barhoumi et al., 2015).

Specifically concerning the reduction of photosynthetic activity due to shading effect, our results showed that cells in contact with IO16 showed similar photosynthetic activity than cells kept apart from NPs (Table 3). This suggests that the decrease in photosynthesis was due to a shading effect in the case of IO16. However, cells without direct contact with IO8 showed less photosynthetic inhibition than the cells in direct contact with the NPs, indicating that part of photosynthesis inhibition was directly caused by IO8 contact (Table 3). Fig. 6 shows chlorophyll *a* content as well as total chlorophyll content (*a* + *b*); as can be observed, both, chlorophyll *a* content as well as total chlorophyll content are significantly reduced by exposure to SPION, these results are in total agreement with those of O_2 evolution reported in Table 3, corroborating the negative effect of SPION on photosynthesis. In the case of IO16, the observed decrease in chlorophyll content was clearly due to shading effect (no significant differences were found between the chlorophyll content of cells in direct contact with SPION *vs.* that of cells not directly exposed to them, $p < 0.05$). However, in the case of IO8, shading inhibited chlorophyll *a* and total chlorophyll content by 30% while those cells in direct contact with the SPION had a significantly ($p < 0.05$) lower chlorophyll content (an inhibition of almost 70% in total chlorophyll content, Fig. 6). Previous works observed a shading effect caused by ZnO, TiO_2 and CuO NPs to *Pseudokirchneriella subcapitata* (*P. subcapitata*) (Aruoja et al., 2009), by carbon nanotubes to *C. vulgaris* and *P. subcapitata* (Schwab et al., 2011), and by Co NPs to the microalgae *Platymonas subcordiforus*, *Chaetoceros curvisetus* and *Skeletonema costatum* (Chen et al., 2018). In line with these studies, the shading effect caused by SPION was probably due to their heteroaggregation with the cells (Fig. S6).

Table 3. Photosynthetic activity (as O2 evolution) of *C. reinhardtii* exposed for 72 h to IO16 and IO8 with and without direct contact (Shading effect) with SPION.

Particle	Control (µmol O_2 mg chl^{-1} h^{-1})	Direct contact (µmol O_2 mg chl^{-1} h^{-1})	Shading effect (µmol O_2 mg chl^{-1} h^{-1})
IO16	143.7 ± 12.0	92.3 ± 17.5	94.0 ± 9.4
IO8	143.7 ± 12.0	68.0 ± 11.9	118.2 ± 29.2

3.6. Effect of SPION in the ultrastructure of *C. reinhardtii* cells and potential internalization

TEM images of *C. reinhardtii* cells after 72 h of exposure to their EC_{50} concentrations are shown in Fig. 7. Fig. 7 A to D show TEM images of non-exposed *C. reinhardtii* with intact ultrastructural morphology,

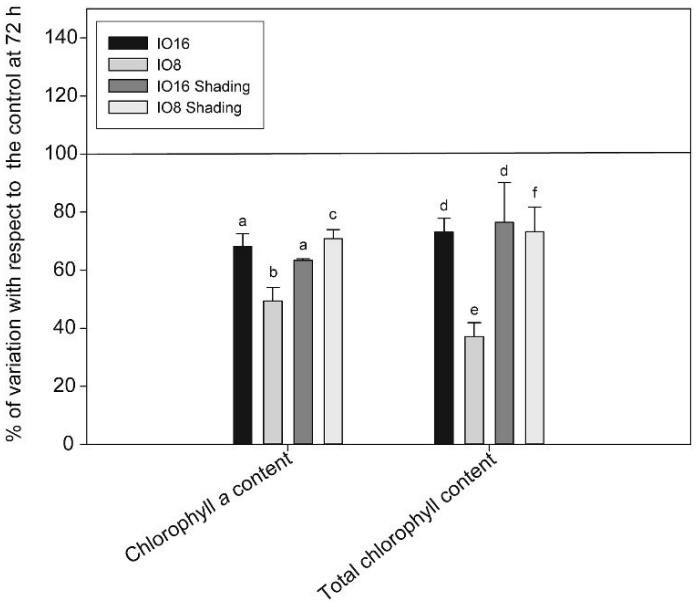

Figure 6. Chlorophyll *a* and total chlorophyll content (a+b) in *C. reinhardtii* after 72 h of exposure to SPION. Results are presented as percentage of variation of each parameter ± SD with respect to control (100% corresponding to the control is indicated by the solid line). Values with the same superscript letter were not significantly different (ANOVA, $p < 0.05$) within each condition assayed.

including cell wall, plasma membrane, chloroplast, pyrenoids, nucleus and other organelles. Fig. 7 F to I and Fig. 7 K to N show TEM images of *C. reinhardtii* exposed to IO16 and IO8, respectively. In both cases, a plasmolysis phenomenon and the presence of many starch grains were observed. Plasmolysis and the formation of starch grains have been previously reported in *C. reinhardtii* exposed to different NPs (Chen et al., 2012a; Martín-de-Lucía et al., 2018). They have been attributed to a self-defense mechanism.

Interestingly, in both cases, the formation of autophagic vacuoles were observed (Fig. 7 F, G, H, K, L, M and N) and was further confirmed by TEM-XEDS that they contained Fe of the SPION (Fig. 7 E, J, O) while no Fe was found in the autophagic vacuoles of unexposed cells (Fig. 7 A). In fact, these autophagic vacuoles containing the SPION might have been originated by fusion with endocytic vesicles engulfing the SPION, perhaps as a detoxifying mechanism (Fig. 6 I, K, L, M and N) (Liou et al., 1997).

Few studies have shown evidence of particle internalization in microalgae using CuO, AgO, CeO_2 or TiO_2 NPs (Chen et al., 2012a; Melegari et al., 2013; Perreault et al., 2012; Taylor et al., 2016; Wang et al., 2016). Particularly, internalization of SPION has been observed in animal cell lines (Calero et al., 2014; Villanueva et al., 2009) but here we show for the first time that SPION can be internalized by microalgae and give ultrastructural evidence (TEM-XEDS) which indicates that endocytosis is the most plausible internalization pathway. Many works have studied the machinery related to endocytosis in higher plants (Irani and Russinova, 2009; Low and Chandra, 1994) However, little is known about this process in algae.

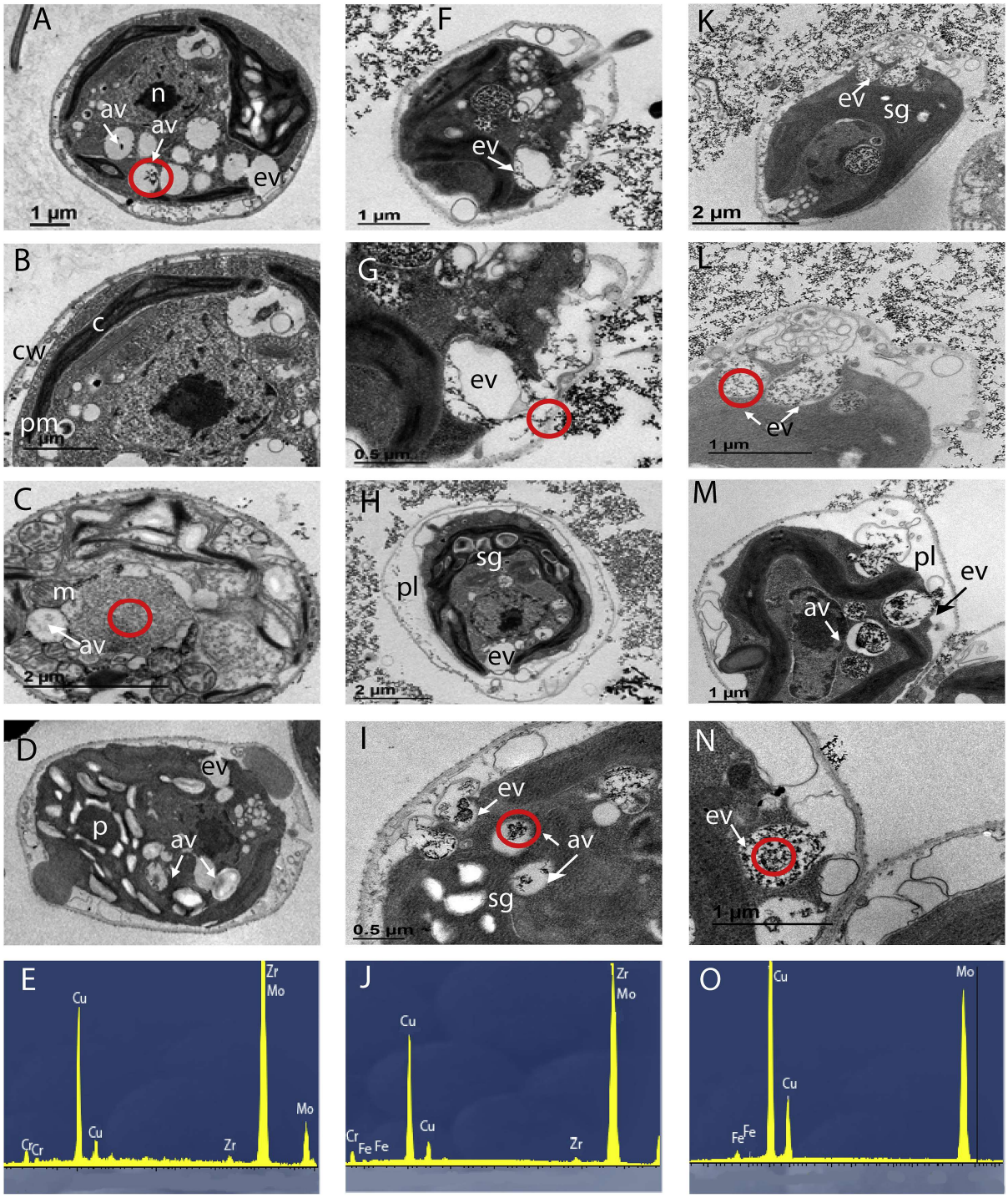

Figure 7. Selected transmission electron microscopy (TEM) images of non-exposed cells (A, B, C, D) accompanied with XEDS spectra (E) and cells exposed to IO16 (F, G, H, I) and IO8 (K, L, M, N) accompanied with XEDS spectra (J, O). cw = cell wall, pm = plasma membrane, n = nucleus, c = chloroplast, m = mitochondria, sg = starch grains, av = autophagic vacuoles, ev = endocytic vesicles pl = plasmolysis. The red circles indicate the location of XEDS spectra.

This study provides novel information on the toxicological mechanisms of SPION in aquatic photosynthetic organisms. Furthermore, the calculated EC_{50} of SPION are lower than those that might be used for site remediation whose potential concentration may oscillate between 2000 and 30,000 mg/L (Yan et al., 2013). These data suggest that SPION might be a potential risk for the aquatic environment if used at such high concentrations and that toxicity assessments with environmental relevant organisms must be done before their use for such applications.

Such as every aerobic organism, *C. reinhardtii* cells are susceptible to suffer oxidative stress. As previously summarized by von Moos and Slaveykova (2014), there exist diverse mechanisms that induce the formation of ROS by NPs. In the present work, one of the main physiological parameters altered was the elevated ROS formation after the exposure to SPION. Elevated ROS production may change membranes permeability, in this regard each SPION caused different alterations; IO8 did not change plasma membrane potential, however IO16 provoked a transient hyperpolarization of the plasma membrane. Moreover, ROS formation triggered lipid peroxidation in both cases, although higher in IO16 case, confirming that the plasma membrane resulted more affected after the exposure to IO16 than after the exposure to IO8. Lipid peroxidation may create pores in the lipid bilayer that might lead to non-specific membrane ion permeability further facilitating the entrance of SPION. These changes in membrane permeability have been described previously by Prado et al. (2012) and Esperanza et al. (2015) after the exposure of *C. reinhardtii* to pollutants such as to paraquat and to atrazine.

Oxidative stress, that may be generated in the mitochondria and other cell locations, is also a mediator of apoptosis and may induce cell death by depolarizing the mitochondrial membrane potential (Ghazizadeh and Nazıroğlu, 2014; González-Pleiter et al., 2017; Uguz et al., 2012). Changes in mitochondria after the exposure and internalization of NPs such as mitochondrial membrane depolarization have been previously reported in animal cell lines (Arvizo et al., 2010; Teodoro et al., 2011).

In this study we observed mitochondrial membrane potential depolarization in the cells after the exposure and internalization of both SPION. This mitochondrial membrane potential depolarization has been previously observed in *C. reinhardtii* after its exposure to different emergent pollutants (González-Pleiter et al., 2017; Martín-de-Lucía et al., 2018; Xia et al., 2006).

Shading effect has been previously seen in microalgae with different NPs causing algal growth inhibition due to impairment of photosynthesis. In our work, we found that one of the most affected parameters of *C. reinhardtii* after exposure to SPION was photosynthesis. This alteration in the photosynthetic system was mostly due to a shading effect in the case of IO16 (explaining almost the 100% of the decrease in photosynthetic activity) but not in the case of IO8 where the shading effect did not explain all the decrease in photosynthesis.

In view of the results presented in this study, after the exposure of *C. reinhardtii* to IO16 and IO8, oxidative stress was caused which triggered many physiological alterations. Furthermore, a decrease in photosynthesis activity was observed mostly by a shading effect. Finally, internalization of the SPION by endocytosis and further sequestering in autophagic vacuoles was observed in *C. reinhardtii*.

4. Conclusions

In conclusion, this is the first time that *C. reinhardtii* has been used as an experimental model to study the effect of SPION. Concerning the SPION concentrations which were toxic for *C. reinhardtii*, we can say that this microalga is, to date, the ecologically relevant organism tested most sensitive to SPION. We found that SPION, over certain concentrations, could be a potential risk for the environment because they inhibited algal growth and induced the production of ROS which derived in an increase in lipid peroxidation. Moreover, SPION also altered the photosynthesis of *C. reinhardtii* by diminishing the access of light as revealed by the shading effects experiments. The internalization of SPION into *C. reinhardtii* has been observed for the first time highlighting the potential effect of these NPs through the trophic chain. The actual SPION concentrations in environment are not clear right now but the concentrations used in some remediation processes are much higher than the concentrations that were toxic for *C. reinhardtii*. Therefore, the use of SPION for site remediation may result in increased concentrations in aquatic environment and their fate and biological effects need to be known before actual damage to the aquatic biota occurs. This study provides valuable information about the potential risks of SPION in the environment and could encourage the study of the toxicity of nanoparticles on environmentally relevant organisms in the future.

Acknowledgements

This research is supported by CTM2013-45775-C2-1/2-R, CTM2016-74927-C2-1,2-R and MAT2015-71806-R grants from MINECO. JHG is working under FPI contract (MINECO-EU).

References

Ahmed, S., 2016. Original research paper biological science estimation of total chlorophyll and total carotenoid contents for strains of *Anabaena* and *Gloeocapsa* through spectrophotometer part time lecturer. Department of Botany. Nagaon Assam KEYW, Dhing College, Dhing, pp. 70-71.

Ambashta, R.D., Sillanpää, M., 2010. Water purification using magnetic assistance: a review. J. Hazard Mater. 180, 38-49.

Arana, I., Orruño, M., Barcina, I., 2009. Cómo abordar y resolver aspectos prácticos de Microbiología, (2009).
Aruoja, V., Dubourguier, H.-C., Kasemets, K., Kahru, A., 2009. Toxicity of nanoparticles of CuO, ZnO and TiO_2 to microalgae *Pseudokirchneriella subcapitata*. Sci. Total Environ. 407, 1461-1468.
Arvizo, R.R., Miranda, O.R., Thompson, M.A., Pabelick, C.M., Bhattacharya, R., Robertson, J.D., et al., 2010. Effect of nanoparticle surface charge at the plasma membrane and beyond. Nano Lett. 10, 2543-2548.
Barhoumi, L., Dewez, D., 2013. Toxicity of superparamagnetic iron oxide nanoparticles on green alga *Chlorella vulgaris*. BioMed Res. Int. 2013.
Barhoumi, L., Oukarroum, A., Taher, L.B., Smiri, L.S., Abdelmelek, H., Dewez, D., 2015. Effects of superparamagnetic iron oxide nanoparticles on photosynthesis and growth of the aquatic plant *Lemna gibba*. Arch. Environ. Contam. Toxicol. 68, 510-520.
Berberoglu, H., Pilon, L., Melis, A., 2008. Radiation characteristics of *Chlamydomonas reinhardtii* CC125 and its truncated chlorophyll antenna transformants tla1, tlaX and tla1-CWþ. Int. J. Hydrogen Energy 33, 6467-6483.
Brookes, J.D., Geary, S.M., Ganf, G.G., Burch, M.D., 2000. Use of FDA and flow cytometry to assess metabolic activity as an indicator of nutrient status in phytoplankton. Mar. Freshw. Res. 51, 817-823.
Bundschuh, M., Filser, J., Lüderwald, S., McKee, M.S., Metreveli, G., Schaumann, G.E., et al., 2018. Nanoparticles in the environment: where do we come from, where do we go to? Environ. Sci. Eur. 30, 6.
Calabrese, E.J., 2016. Preconditioning is hormesis part I: documentation, dose-response features and mechanistic foundations. Pharmacol. Res. 110, 242-264.
Calabrese, E.J., Baldwin, L.A., 2001. Hormesis: U-shaped dose responses and their centrality in toxicology. Trends Pharmacol. Sci. 22, 285-291.
Calero, M., Gutiérrez, L., Salas, G., Luengo, Y., Lázaro, A., Acedo, P., et al., 2014. Efficient and safe internalization of magnetic iron oxide nanoparticles: two fundamental requirements for biomedical applications. Nanomed. Nanotechnol. Biol. Med. 10, 733-743.
Cid, A., Fidalgo, P., Herrero, C., Abalde, J., 1996. Toxic action of copper on the membrane system of a marine diatom measured by flow cytometry. Cytometry: The Journal of the International Society for Analytical Cytology 25, 32-36.
Cui, H.-J., Shi, J.-W., Yuan, B., Fu, M.-L., 2013. Synthesis of porous magnetic ferrite nanowires containing Mn and their application in water treatment. J. Mater. Chem. 1, 5902-5907.
Chen, L., Zhou, L., Liu, Y., Deng, S., Wu, H., Wang, G., 2012a. Toxicological effects of nanometer titanium dioxide (nano-TiO_2) on *Chlamydomonas reinhardtii*. Ecotoxicol. Environ. Saf. 84, 155-162.
Chen, X., Zhang, C., Tan, L., Wang, J., 2018. Toxicity of Co nanoparticles on three species of marine microalgae. Environ. Pollut. 236, 454-461.
Chen, X., Zhu, X., Li, R., Yao, H., Lu, Z., Yang, X., 2012b. Photosynthetic toxicity and oxidative damage induced by nano-Fe_3O_4 on *Chlorella vulgaris* in aquatic environment. Open J. Ecol. 2, 21.
Deryabin, D., Aleshina, E., 2008. Effect of salts on luminescence of natural and recombinant luminescent bacterial biosensors. Appl. Biochem. Microbiol. 44, 292-296.
Elbaz, A., Wei, Y.Y., Meng, Q., Zheng, Q., Yang, Z.M., 2010. Mercury-induced oxidative stress and impact on antioxidant enzymes in *Chlamydomonas reinhardtii*.
Ecotoxicology 19, 1285-1293.
Esperanza, M., Seoane, M., Rioboo, C., Herrero, C., Cid, A., 2015. *Chlamydomonas reinhardtii* cells adjust the metabolism to maintain viability in response to atrazine stress. Aquat. Toxicol. 165, 64-72.
Fadeel, B., Garcia-Bennett, A.E., 2010. Better safe than sorry: understanding the toxicological properties of inorganic nanoparticles manufactured for biomedical applications. Adv. Drug Deliv. Rev. 62, 362-374.
Forbes, V.E., 2000. Is hormesis an evolutionary expectation? Funct. Ecol. 14, 12-24.
Ghazizadeh, V., Nazıroglu, M., 2014. Electromagnetic radiation (Wi-Fi) and epilepsy induce calcium entry and apoptosis through activation of TRPV1 channel in
hippocampus and dorsal root ganglion of rats. Metab. Brain Dis. 29, 787-799.
Gholami, A., Rasoul-amini, S., Ebrahiminezhad, A., Seradj, S.H., Ghasemi, Y., 2015. Lipoamino acid coated superparamagnetic iron oxide nanoparticles concentration and time dependently enhanced growth of human hepatocarcinoma cell line (Hep-G2). J. Nanomater. 16, 150.
González-Pleiter, M., Rioboo, C., Reguera, M., Abreu, I., Leganés, F., Cid, A., et al., 2017. Calcium mediates the cellular response of *Chlamydomonas reinhardtii* to the
emerging aquatic pollutant Triclosan. Aquat. Toxicol. 186, 50-66.
Gonzalo, S., Llaneza, V., Pulido-Reyes, G., Fernandez-Piñas, F., Bonzongo, J.C., Leganés, F., et al., 2014. A colloidal singularity reveals the crucial role of colloidal stability for nanomaterials in-vitro toxicity testing: nZVI-microalgae colloidal system as a case study. PLoS One 9, e109645.
Gutiérrez, A.M., Dziubla, T.D., Hilt, J.Z., 2017. Recent advances on iron oxide magnetic nanoparticles as sorbents of organic pollutants in water and wastewater treatment. Rev. Environ. Health 32, 111-117.

Hoober, J.K., 1989. The *Chlamydomonas* sourcebook: a comprehensive guide to biology and laboratory use. Science 246, 1503-1505.
Hu, J., Chen, G., Lo, I.M., 2005. Removal and recovery of Cr (VI) from wastewater by maghemite nanoparticles. Water Res. 39, 4528-4536.
Irani, N.G., Russinova, E., 2009. Receptor endocytosis and signaling in plants. Curr. Opin. Plant Biol. 12, 653-659.
Khin, M.M., Nair, A.S., Babu, V.J., Murugan, R., Ramakrishna, S., 2012. A review on nanomaterials for environmental remediation. Energy Environ. Sci. 5,
8075-8109.
Laffon, B., Fernández-Bertólez, N., Costa, C., Brandão, F., Teixeira, J.P., Pásaro, E., et al., 2018. Cellular and molecular toxicity of iron oxide nanoparticles. Cellular and Molecular Toxicology of Nanoparticles. Springer, pp. 199-213.
Leganés, F., Martínez-Granero, F., Muñoz-Martín, M.A., Marco, E., Jorge, A., Carvajal, L., et al., 2014. Characterization and responses to environmental cues
of a photosynthetic antenna-deficient mutant of the filamentous cyanobacterium *Anabaena* sp. PCC 7120. J. Plant Physiol. 171, 915-926.
Liou, W., Geuze, H.J., Geelen, M.J., Slot, J.W., 1997. The autophagic and endocytic pathways converge at the nascent autophagic vacuoles. J. Cell Biol. 136, 61-70.
Low, P.S., Chandra, S., 1994. Endocytosis in plants. Annu. Rev. Plant Biol. 45, 609-631.
Llaneza, V., Rodea-Palomares, I., Zhou, Z., Rosal, R., Fernandez-Pina, F., Bonzongo, J.C., 2016. Polyvinylpyrrolidone and arsenic-induced changes in biological responses of model aquatic organisms exposed to iron-based nanoparticles. J. Nanoparticle Res. 18, 235.
Martín-de-Lucía, I., Campos-Mañas, M.C., Agüera, A., Leganés, F., Fernández-Piñas, F., Rosal, R., 2018. Combined toxicity of graphene oxide and wastewater to the green alga Chlamydomonas reinhardtii. Environ. Sci.: Nano 5 (7), 1729-1744.
Matei, E., Predescu, A.M., Coman, G., Balanescu, M., Sohaciu, M., Predescu, C., et al., 2016. Magnetic nanoparticles used in environmental engineering for Pb and Zn removal. Environmental Engineering & anagement Journal (EEMJ) 15.
Melegari, S.P., Perreault, F., Costa, R.H.R., Popovic, R., Matias, W.G., 2013. Evaluation of toxicity and oxidative stress induced by copper oxide nanoparticles in the green alga Chlamydomonas reinhardtii. Aquat. Toxicol. 142, 431-440.
Mosayebi, J., Kiyasatfar, M., Laurent, S., 2017. Synthesis, functionalization, and design of magnetic nanoparticles for theranostic applications. Adv. Healthc. Mater. 6, 1700306.
Navarro, E., Piccapietra, F., Wagner, B., Marconi, F., Kaegi, R., Odzak, N., et al., 2008. Toxicity of silver nanoparticles to *Chlamydomonas reinhardtii*. Environ. Sci. Technol. 42, 8959-8964.
Navarro, E., Wagner, B., Odzak, N., Sigg, L., Behra, R., 2015. Effects of differently coated silver nanoparticles on the photosynthesis of *Chlamydomonas reinhardtii*. Environ. Sci. Technol. 49, 8041-8047.
Ortega-Villasante, C., Rellán-Álvarez, R., Del Campo, F.F., Carpena-Ruiz, R.O., Hernández, L.E., 2005. Cellular damage induced by cadmium and mercury in
Medicago sativa. J. Exp. Bot. 56, 2239-2251.
Pacakova, B., Kubickova, S., Salas, G., Mantlikova, A., Marciello, M., Morales, M., et al., 2017. The internal structure of magnetic nanoparticles determines the magnetic response. Nanoscale 9, 5129-5140.
Park, J., An, K., Hwang, Y., Park, J.-G., Noh, H.-J., Kim, J.-Y., et al., 2004. Ultra-largescale syntheses of monodisperse nanocrystals. Nat. Mater. 3, 891.
Parsons, P.A., 2003. Metabolic efficiency in response to environmental agents predicts hormesis and invalidates the linear no-threshold premise: ionizing radiation as a case study. Crit. Rev. Toxicol. 33, 443e449.
Perreault, F., Oukarroum, A., Melegari, S.P., Matias, W.G., Popovic, R., 2012. Polymer coating of copper oxide nanoparticles increases nanoparticles uptake and toxicity in the green alga *Chlamydomonas reinhardtii*. hemosphere 87, 1388-1394.
Prado, R., Rioboo, C., Herrero, C., Suárez-Bregua, P., Cid, A., 2012. Flow cytometric analysis to evaluate physiological alterations in herbicide-exposed *Chlamydomonas moewusii* cells. Ecotoxicology 21, 409-420.
Pulido-Reyes, G., Rodea-Palomares, I., Das, S., Sakthivel, T.S., Leganés, F., Rosal, R., et al., 2015. Untangling the biological effects of cerium oxide nanoparticles: the role of surface valence states. Sci. Rep. 5, 15613.
Rodea-Palomares, I., Boltes, K., Fernández-Piñas, F., Leganés, F., García-Calvo, E., Santiago, J., et al., 2010. Physicochemical characterization and ecotoxicological
assessment of CeO_2 nanoparticles using two aquatic microorganisms. Toxicol. Sci. 119, 135-145.
Rodea-Palomares, I., Gonzalo, S., Santiago-Morales, J., Leganes, F., García-Calvo, E., Rosal, R., et al., 2012. An insight into the mechanisms of nanoceria toxicity in
aquatic photosynthetic organisms. Aquat. Toxicol. 122, 133-143.
Saison, C., Perreault, F., Daigle, J.-C., Fortin, C., Claverie, J., Morin, M., et al., 2010. Effect of core-shell copper oxide nanoparticles on cell culture morphology and photosynthesis (photosystem II energy distribution) in the green alga, *Chlamydomonas reinhardtii*. Aquat. Toxicol. 96, 109-114.

Salas, G., Casado, C., Teran, F.J., Miranda, R., Serna, C.J., Morales, M.P., 2012. Controlled synthesis of uniform magnetite nanocrystals with high-quality properties for biomedical applications. J. Mater. Chem. 22, 21065-21075.

Saptarshi, S.R., Duschl, A., Lopata, A.L., 2013. Interaction of nanoparticles with proteins: relation to bio-reactivity of the nanoparticle. J. Nanobiotechnol. 11, 26.

Schwab, F., Bucheli, T.D., Lukhele, L.P., Magrez, A., Nowack, B., Sigg, L., et al., 2011. Are carbon nanotube effects on green algae caused by shading and agglomeration? Environ. Sci. Technol. 45, 6136e6144.

Ševců, A. El-Temsah, Y.S., Joner, E.J., Cerník, M., 2009. Oxidative stress induced in microorganisms by zero-valent iron nanoparticles. Microb. Environ. 1107220320-1107220320.

Sheikh, M.H., 2013. Separation of Copper-Oxide Nanoparticles from Nanoparticle Enhanced Phase Change Material. University of Alabama Libraries.

Singh, N., Jenkins, G.J., Asadi, R., Doak, S.H., 2010. Potential toxicity of superparamagnetic iron oxide nanoparticles (SPION). Nano Rev. 1, 5358.

Stebbing, A., 1997. A theory for growth hormesis. Belle Newsletter 6.

Sun, S., Zeng, H., Robinson, D.B., Raoux, S., Rice, P.M., Wang, S.X., et al., 2004. Monodisperse MFe_2O_4 (M = Fe, Co, Mn) nanoparticles. J. Am. Chem. Soc. 126, 273-279

Tamayo-Belda, M., González-Pleiter, M., Pulido-Reyes, G., Martin-Betancor, K., Leganés, F., Rosal, R., et al., 2019. Mechanism of the toxic action of cationic G5 and G7 PAMAM dendrimers in the cyanobacterium *Anabaena* sp. PCC7120. Environ. Sci.: Nano 6, 863-878.

Tang, S.C., Lo, I.M., 2013. Magnetic nanoparticles: essential factors for sustainable environmental applications. Water Res. 47, 2613-2632.

Taylor, N.S., Merrifield, R., Williams, T.D., Chipman, J.K., Lead, J.R., Viant, M.R., 2016. Molecular toxicity of cerium oxide nanoparticles to the freshwater alga *Chlamydomonas reinhardtii* is associated with supra-environmental exposure concentrations. Nanotoxicology 10, 32-41.

Teodoro, J.S., Simoes, A.M., Duarte, F.V., Rolo, A.P., Murdoch, R.C., Hussain, S.M., et al. 2011. Assessment of the toxicity of silver nanoparticles *in vitro*: a mitochondrial perspective. Toxicol. In Vitro 25, 664-670.

Tong, M., Yuan, S., Long, H., Zheng, M., Wang, L., Chen, J., 2011. Reduction of nitrobenzene in groundwater by iron nanoparticles immobilized in PEG/nylon membrane. J. Contam. Hydrol. 122, 16-25.

Truskewycz, A., Patil, S., Ball, A., Shukla, R., 2018. Iron Nanoparticles for Contaminated Site Remediation and Environmental Preservation. Nanobiotechnology. CRC Press, pp. 323-373.

Uguz, A.C., Cig, B., Espino, J., Bejarano, I., Naziroglu, M., Rodríguez, A.B., et al., 2012. Melatonin potentiates chemotherapy-induced cytotoxicity and apoptosis in rat pancreatic tumor cells. J. Pineal Res. 53, 91-98.

Villanueva, A., Canete, M., Roca, A.G., Calero, M., Veintemillas-Verdaguer, S., Serna, C.J., et al., 2009. The influence of surface functionalization on the enhanced internalization of magnetic nanoparticles in cancer cells. Nanotechnology 20, 115103.

von Moos, N., Maillard, L., Slaveykova, V.I., 2015. Dynamics of sub-lethal effects of nano-CuO on the microalga *Chlamydomonas reinhardtii* during short-term exposure. Aquat. Toxicol. 161, 267-275.

von Moos, N., Slaveykova, V.I., 2014. Oxidative stress induced by inorganic nanoparticles in bacteria and aquatic microalgae state of the art and knowledge gaps. Nanotoxicology 8, 605-630.

Wang, J., Zhang, X., Chen, Y., Sommerfeld, M., Hu, Q., 2008. Toxicity assessment of manufactured nanomaterials using the unicellular green alga *Chlamydomonas reinhardtii*. Chemosphere 73, 1121-1128.

Wang, S., Lv, J., Ma, J., Zhang, S., 2016. Cellular internalization and intracellular biotransformation of silver nanoparticles in *Chlamydomonas reinhardtii*. Nanotoxicology 10, 1129-1135.

Wu, Q., Li, Y., Tang, M., Wang, D., 2012. Evaluation of environmental safety concentrations of DMSA coated Fe_2O_3-NPs using different assay systems in nematode Caenorhabditis elegans. PLoS One 7, e43729.

Xia, T., Kovochich, M., Brant, J., Hotze, M., Sempf, J., Oberley, T., et al., 2006. Comparison of the abilities of ambient and manufactured nanoparticles to induce cellular toxicity according to an oxidative stress paradigm. Nano Lett. 6, 1794-1807.

Yan, W., Lien, H.-L., Koel, B.E., Zhang, W.X., 2013. Iron nanoparticles for environmental clean-up: recent developments and future outlook. Environ. Sci.: Processes & Impacts 15, 63-77.

Yavuz, C.T., Mayo, J., William, W.Y., Prakash, A., Falkner, J.C., Yean, S., et al., 2006. Low-field magnetic separation of monodisperse Fe_3O_4 nanocrystals. Science 314, 964-967.

Zhang, S., Niu, H., Cai, Y., Shi, Y., 2010. Barium alginate caged Fe_3O_4@ C18 magnetic nanoparticles for the pre-concentration of polycyclic aromatic hydrocarbons and phthalate esters from environmental water samples. Anal. Chim. Acta 665, 167-175.

Zhang, Wx, Elliott, D.W., 2006. Applications of iron nanoparticles for groundwater remediation. Remediat. J. 16, 7-21.

SUPPLEMENTARY MATERIAL

Toxicity of superparamagnetic iron oxide nanoparticles to the microalga *Chlamydomonas reinhardtii*

JaraHurtado-Gallego[1], GerardoPulido-Reyes[1], MiguelGonzález-Pleiter[1], GorkaSalas[2], FranciscoLeganés[1], RobertoRosal[3] FranciscaFernández-Piñas[1,*]

[1] Departamento de Biología, Universidad Autónoma de Madrid, Cantoblanco, E-28049 Madrid, Spain
[2] IMDEA Nanociencia, C/Faraday 9, Cantoblanco, 28049 Madrid, Spain
[3] Departamento de Ingeniería Química, Universidad de Alcalá, E-28871 Alcalá de Henares, Madrid, Spain
[*] Corresponding author: francisca.pina@uam.es

Contents

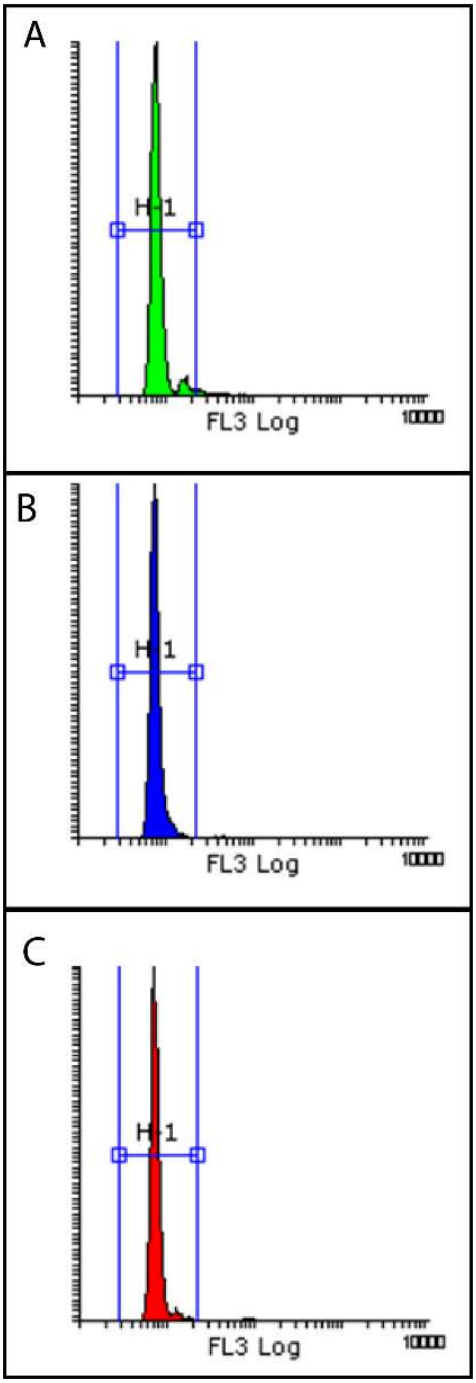

Figure S1. Effect of SPION (after 72 h of exposure) on cell membrane integrity of *C. reinhardtii* by FCM using the fluorochrome PI. Histograms show the distribution of fluorescence intensity of PI (Y-axis: cell number, X-axis: fluorescence intensity in arbitrary units, a.u.). A) Unexposed cells in TAP/6 growth medium (PI data of cells in TAP growth medium without dilution were identical) ,B) cells after 72 h of exposure to IO16 and C) cells after 72 h of exposure to IO8. H1 region represents cell subpopulations comprising intact cell (PI^-).

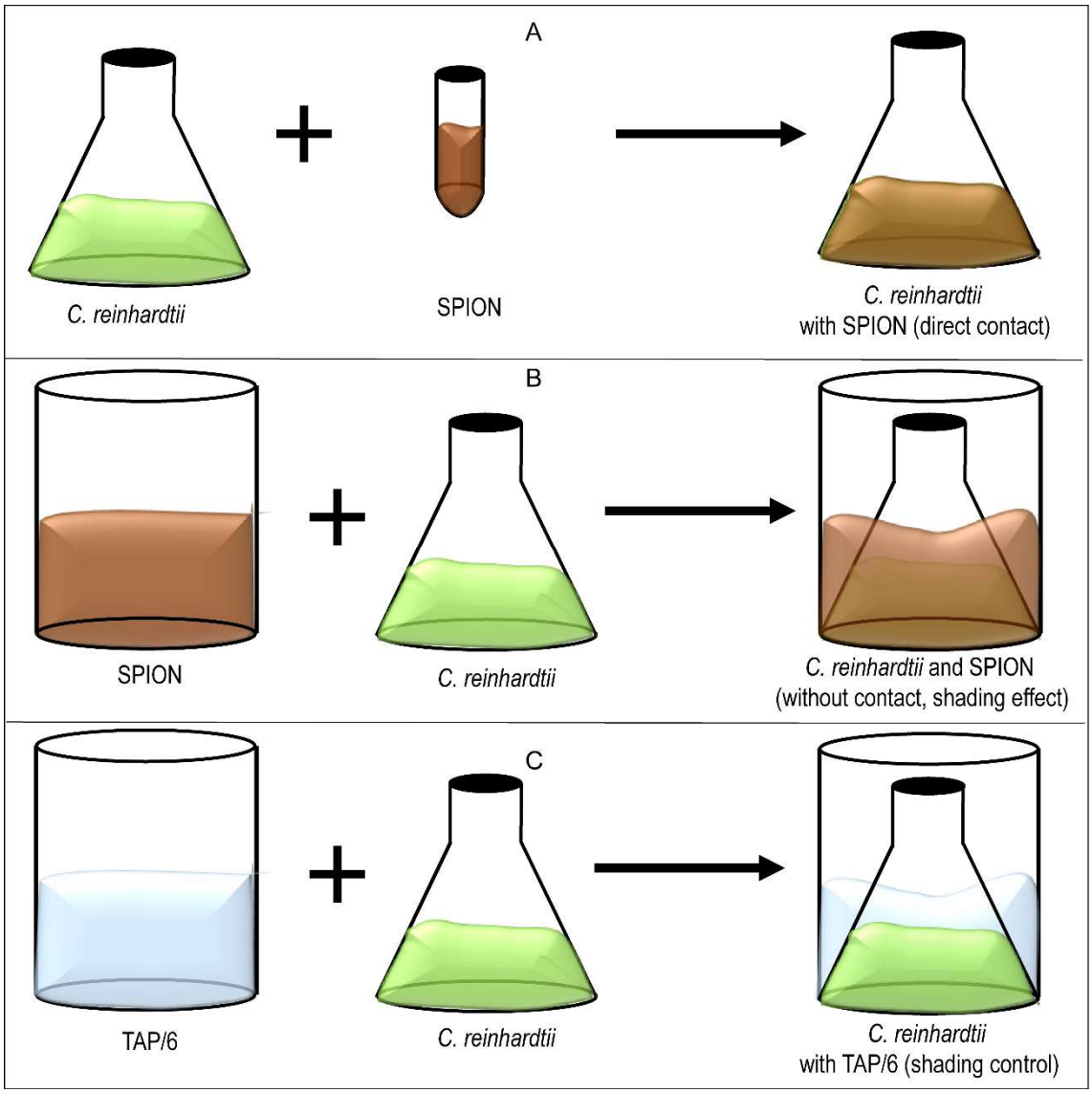

Figure S2. Representative illustration of shading effect experiments. A, represents the regular toxicity assays, where *C. reinhardtii* is exposed to SPION in direct contact. B, represents the shading effect experiments, where *C. reinhardtii* is not in direct contact with the SPION. C represents the control (untreated cells) in the shading experiments.

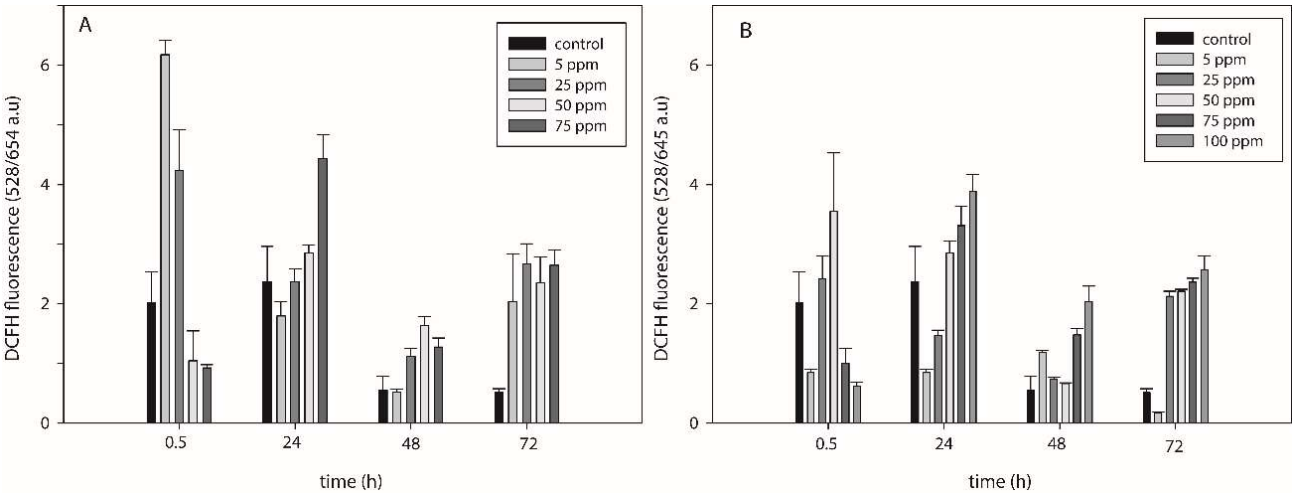

Figure S3. Effect of SPION on intracellular ROS production of *C. reinhardtii* using the fluorochrome H_2DCFDA after 0.5, 24, 48 and 72 h of exposure. H_2DCFDA fluorescence is expressed as arbitrary units (a.u) ± SD. A, represents ROS production of *C. reinhardtii* after the exposure to IO16 and B represents ROS production of *C. reinhardtii* after the exposure to IO8.

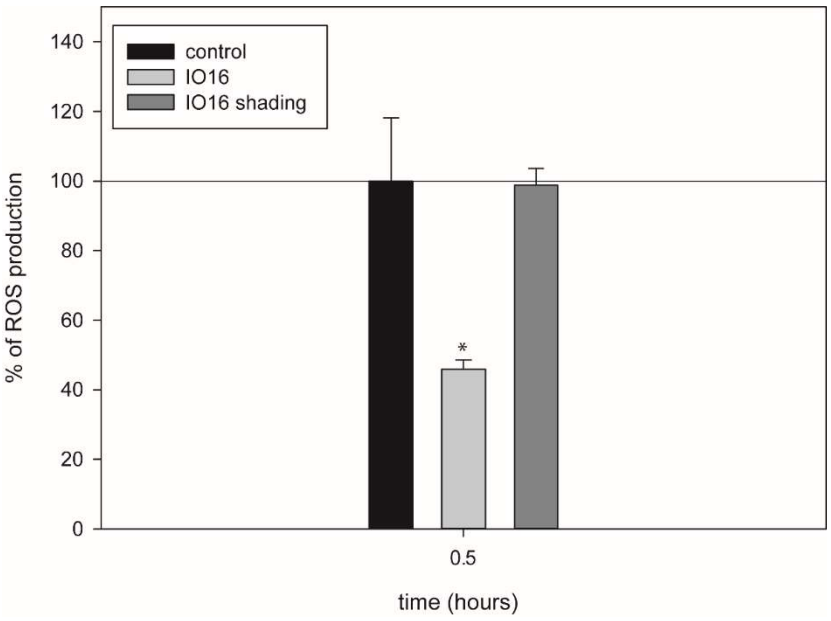

Figure S4. Effect of IO16 with and without contact (shading effect) on intracellular ROS production of *C. reinhardtii* cells using the fluorochrome H_2DCFDA after 30 minutes of exposure. Results are presented as percentage ± SD with respect to the control (100% as indicated by the solid line). Asterisks indicate statistically significant (* $p < 0.05$) differences.

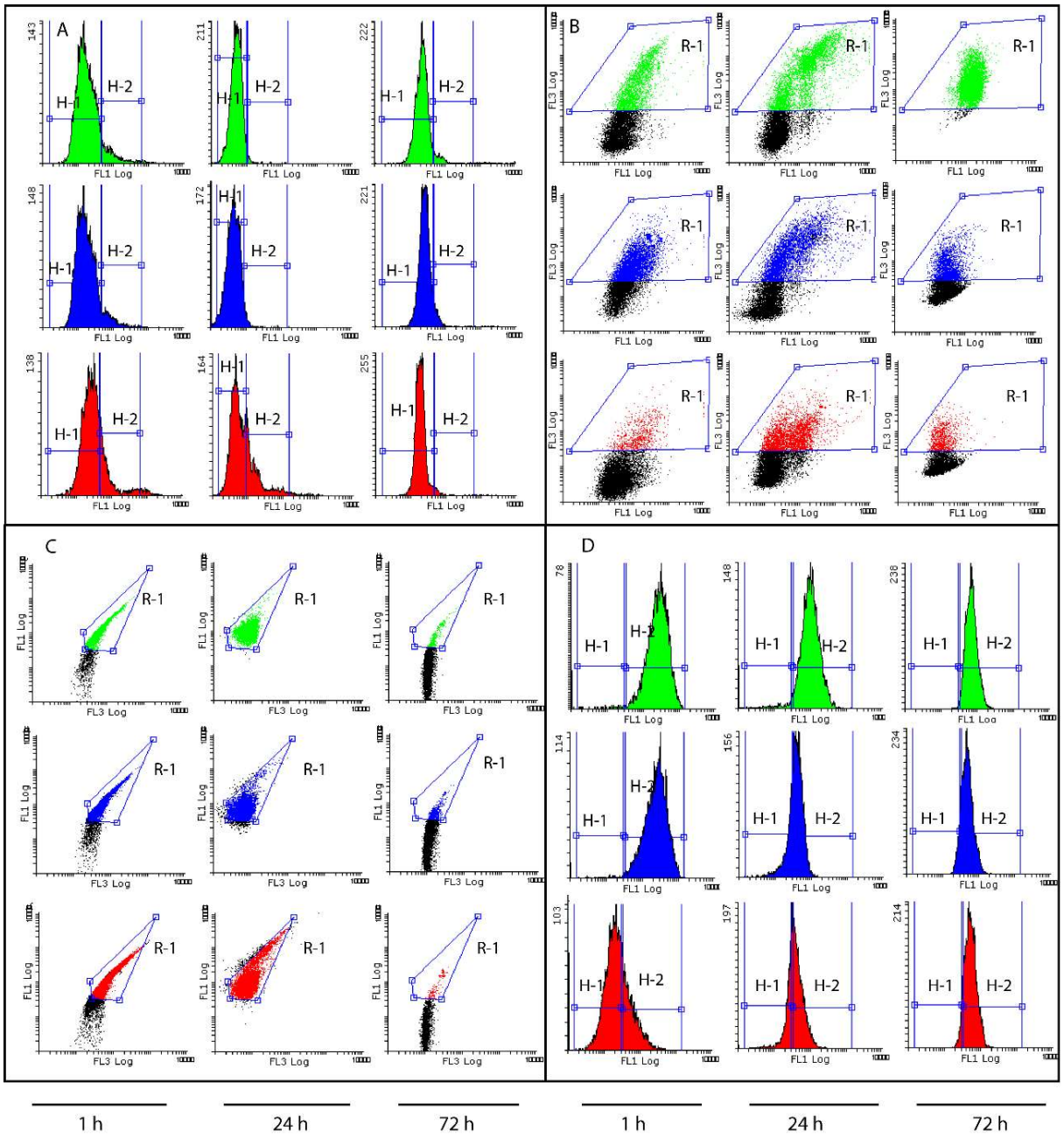

Figure S5. Flow cytometry analysis of physiological parameters after 1, 24 and 72 h of exposure of *C. reinhardtii* to SPION. Representative results of the different fluorochromes which measure (A) plasma membrane potential, (B) mitochondrial membrane potential, (C) intracellular pH and (D) metabolic activity. A and D are represented as histograms where Y-axis represent cell number and X-axis represent fluorescence intensity in arbitrary units, a.u. The changes in the fluorescence intensity are observed along the X-axis. B and C are shown as dot plots where Y- axis and X- axis represents FL3 and FL1 in C and FL1 and FL 3 in D respectively. In both cases (B and C) R-1 represents the cellular subpopulations affected by exposure to SPION. In all cases, control is represented in green, IO16 in blue and IO8 in red.

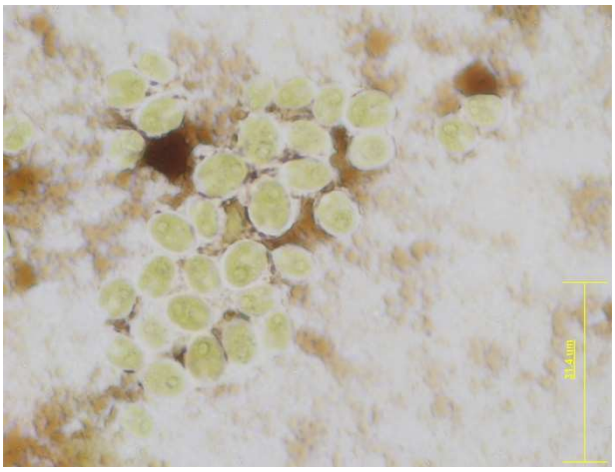

Figure S6. Bright-field micrograph of *C. reinhardtii* where the effect of heteroaggregation of SPION with the cells is observed.